Available online at www.sciencedirect.com
SCIENCE DIRECT
Catalysis Today 111 (2006) 164–170
CATALYSIS TODAY
www.elsevier.com/locate/cattod

The $CO–H_2$ and $CO–H_2O$ reactions over TiO_2 nanotubes filled with Pt metal nanoparticles

Yasushi Sato, Makiko Koizumi, Toshihiro Miyao, Shuichi Naito *

Department of Applied Chemistry, Faculty of Engineering, Kanagawa University, 3-27-1, Rokkakubashi, Kanagawa-ku, Yokohama 221-8686, Japan

Available online 15 December 2005

Abstract

We have investigated the catalytic behavior of Pt encapsulated TiO_2 nanotubes for the water gas shift reaction as well as the hydrogenation of CO. Pt–TiO_2 nanotube catalysts were prepared by employing fine fiber shaped crystals of $[Pt(NH_3)_4](HCO_3)_2$ complex as a structure determining template material. The turnover frequencies (TOF) of these nanotube catalysts were more than one order of magnitude larger than conventional impregnation Pt/TiO_2 catalysts, and the selectivity for methanol in $CO–H_2$ reaction was extraordinary high compared to the impregnation catalysts. The XPS and XRD analyses of the nanotubes revealed characteristic electronic state of reduced TiO_2 (Ti^{3+} in rutile structure) with zerovalent Pt even after the calcination at 773 K. In WGS reaction, electron rich Ti^{3+} on the nanotube wall may play an important role to activate water molecules for the oxidation of CO. In $CO–H_2$ reaction, similar promotion effect of Ti^{3+} species may be operating for selective methanol formation by supplying active OH(a).

Keywords: Water gas shift reaction; CO hydrogenation; Pt–TiO_2 nanotube; Methanol; Pt nanoparticle; Pt nanocluster

1. Introduction

The synthesis of a material with a well-defined nanoscale cavity has been currently under intensive investigation because of its potential utility as adsorbents, electron devices and catalysts [1]. However, little is known yet about the property of these nano-cavities as a catalytic reactor. Recently we have succeeded in the preparation of silica nanotubes and nanocapsules, by employing fiber shaped or rectangular shaped nano-crystals of group VIII metal ammine complexes as a structure determining template material [2]. By hydrolyzing tetraethoxysilane (TEOS) selectively around the surface of these crystals, hollow SiO_2 nanotubes or nanocapsules were formed after higher temperature treatments. By substituting alcohoxide from TEOS to aluminium and titanium isopropoxide, we could synthesize alumina and titania nanocomposites by the same procedures [3].

In the case of silica supported nanocomposite materials, unique selective gas permeation property was observed. We have investigated the adsorption behavior of H_2 and CO over these nanocomposite materials and found a marked stabilization effect of adsorbed hydrogen over the metals in the network of silica wall and inside nanoscale cavities [2]. On the other hand, in the case of titania nanocomposites we have succeeded in the preparation of Pt nanotube and Ir and Rh nanocapsules, which showed no selective adsorption of CO and H_2, but exhibited unique catalytic behavior for water gas shift as well as CO hydrogenation reactions.

The water gas shift reaction (WGS reaction) has been applied to increase the hydrogen production for the synthesis of ammonia. Since it is moderately exothermic, the reaction is industrially achieved in two steps namely, at 623–723 K, the high temperature shift (HTS), and at 453–503 K, the low temperature shift (LTS). More recently, the interest on the WGS reaction has been renewed for application to fuel processing for fuel cell-power generation. Advanced LTS catalysts are needed to produce essentially CO-free hydrogen to feed the PEM fuel cells under development for automobiles. Desired catalyst characteristics include high activity and stability over a wider

* Corresponding author. Tel.: +81 45 481 5661x3903; fax: +81 45 491 7915.
E-mail address: naitos01@kanagawa-u.ac.jp (S. Naito).

0920-5861/$ – see front matter © 2005 Elsevier B.V. All rights reserved.
doi:10.1016/j.cattod.2005.10.020

operating temperature window than is currently possible with the commercial LTS catalysts.

In the present study, we have compared the catalytic behavior of Pt–TiO_2(nt) catalysts in the WGS reaction and CO–H_2 reaction with conventional impregnated Pt/TiO_2(imp) catalysts to elucidate the role of tube structures in these reactions. In situ FT-IR spectroscopy as well as kinetical investigation were applied to study the mechanism of these reactions.

2. Experimental

2.1. Preparation of catalysts

Pt encapsulated TiO_2 nanotube was prepared by a modified method of Hippe et al. [4,5]; first of all, re-crystallization of $[Pt(NH_3)_4](HCO_3)_2$ complexes was carried out by adding isopropanol to the saturated aqueous solution of the complexes, which gave fine fiber-shaped nanocrystals. Then isopropanol solution of tetraisopropyl-orthotitanate (TIPT) was added to this solution and stirred at room temperature for 72 h to hydrolyze TIPT selectively on the surface of the fiber complex crystals. After removal of the solvent, white precipitate-gel was calcined at 773 K and black fine powders of Pt–TiO_2 nanotube was obtained.

Conventional impregnation catalyst (3 wt.% Pt/TiO_2) was prepared by employing H_2PtCl_6 as precursors onto commercial TiO_2 support (CS-300S-12, Sakai chemicals).

2.2. Procedure of catalytic reactions

The catalytic reaction was carried out in a closed gas circulation system with the online gas chromatography (TCD and FID). The Pt–TiO_2(nt) or 3 wt.% Pt/TiO_2(imp) catalyst (0.1 g) was put in a U-shaped reaction vessel which was connected to the circulation system and reduced by 200 Torr of H_2 at 573 K for 5 h before reaction. The water gas shift reaction was carried out with an equimolar amount of CO and H_2O (10 Torr each) at around 373 K, and CO hydrogenation with 1:2 ratio of CO and H_2 (total: 90 Torr) at 423 K.

2.3. Characterization of catalysts

A transmission electron microscope (JEM2010, JEOL) with an acceleration voltage of 200 kV and LaB_6 cathode was applied for the observation of the images of supported catalysts. Samples were prepared by suspending the catalyst powder ultrasonically in 2-propanol and depositing a drop of the suspension on a standard copper grid covered with carbon monolayer film. A X-ray photoelectron spectroscopy (JPS-9010, JEOL) with Mg Kα X-ray source (10 kV, 10 mA) was applied for the analysis of the electronic states of supported catalysts. Samples were prepared by molding in thin disk shape and etched by accelerated Ar ion beam for 30 s. The amount of hydrogen and CO adsorption was measured by a static volumetric adsorption apparatus (Omnisorp100CX, Beckmann Coulter) at room temperature and used for TOF estimation.

3. Results and discussion

3.1. Characterization of Pt–TiO_2(nt)

Fig. 1 shows TEM images of the formed nanotube catalysts, whose shapes are determined by the crystal shapes of the template complexes. The thickness of the TiO_2 wall depended on the hydrolysis period. After 30 min hydrolysis at room temperature the wall of TiO_2 tube was rather thin, but it became thicker by prolonging the hydrolysis period. After 45 h of hydrolysis, obtained tube's ends were mostly closed with a diameter of 100–200 nm, length of 400–1000 nm and wall thickness of 10–20 nm. By EDX analysis, the black part of the inner wall surface was recognized to be aggregated Pt nanoparticles formed by the decomposition of the template complexes during heat treatment. Tiny Pt clusters (0.3–0.5 nm) were also observed in the network of TiO_2 walls. From the elemental analysis, the tube contains about 30 wt.% of Pt metal, and adsorption measurements of H_2 and CO exhibited that the average Pt dispersion was 0.09 in the nanotube catalyst (Table 1). The role of these Pt metal species for the catalytic reactions will be discussed later.

Fig. 2(a) represents the XRD analysis of the prepared Pt–TiO_2 nanotube, where the crystalline structure of the calcined

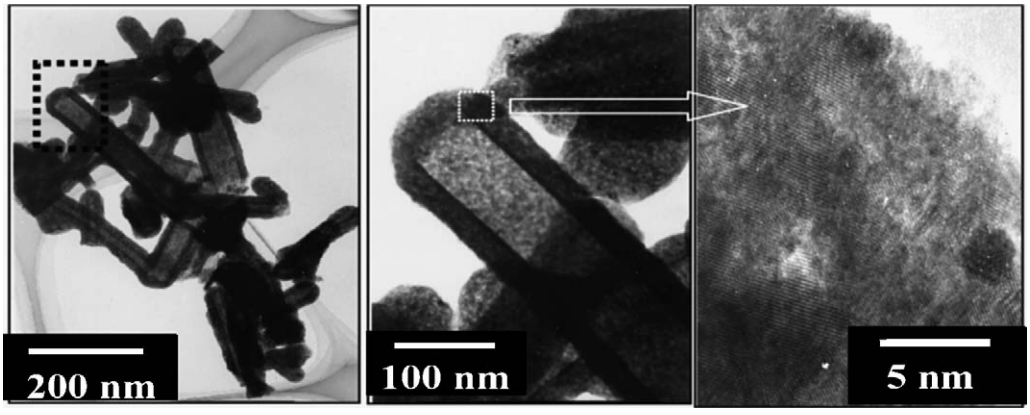

Fig. 1. TEM images of Pt–TiO_2 nanotube catalyst.

Table 1
Amount of adsorption and dispersion of Pt–TiO_2(nt) and Pt/TiO_2(imp)

Catalysts	Hydrogen		Carbon monoxide	
	μmol/g_{cat}	Dispersion	μmol/g_{cat}	Dispersion
Pt–TiO_2(nt)	88.8	0.09	171	0.09
Pt/TiO_2(imp)	58.9	0.16	441	0.58

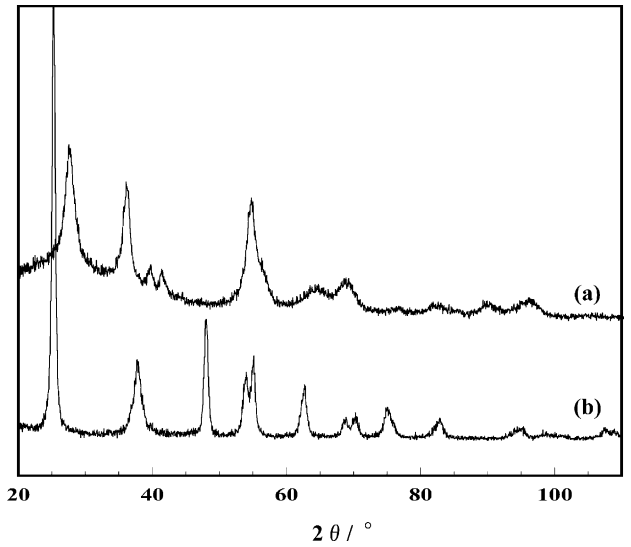

Fig. 2. XRD patterns: (a) Pt–TiO_2(nt) and (b) TiO_2 prepared from TIPT only.

sample was only rutile. On the contrary, TiO_2 sample prepared from the similar hydrolysis method of TIPT without $Pt(NH_3)_6(HCO_3)_2$ complexes showed completely anatase structure as shown in Fig. 2(b). Accordingly Pt ammine complexes may play some unique role for the formation of rutile structure during the hydrolysis process.

Fig. 3 represents the comparison of XPS analyses between Pt–TiO_2(nt) and Pt/TiO_2(imp). The binding energy of Pt $4f_{7/2}$ in nanotube (71.2 eV) was close to the zerovalent Pt (71.0 eV), but impregnated Pt was slightly positively charged (71.7 eV). On the contrary, the binding energy of Ti $2p_{3/2}$ in Pt/TiO_2 (imp) was nearly Ti^{4+} value (459.1 eV), but that of nanotube was close to the value of Ti^{3+}(458.1 eV). These results suggest that the electronic circumstance of Pt nanoparticles inside the TiO_2 nanotube is quite different from Pt over TiO_2 outersurface.

Table 1 summarizes the results of H_2 and CO adsorption at room temperature over Pt–TiO_2 nanotube and impregnated Pt/TiO_2 employed in this study. In the case of nanotube the amount of adsorbed H(a) and CO(a) was the same, from which the dispersion was estimated to be 0.09 and the average particle size of Pt about 10 nm. As mentioned already, there exists smaller Pt clusters in the network of TiO_2, the particle sizes of the aggregated Pt on the inner surface of TiO_2 tubes should be bigger than 10 nm. On the other hand, in the case of impregnated catalysts the amount of adsorbed hydrogen was much less than that of CO, which corresponds well to the XPS analysis that the binding energy of Pt in impregnated Pt/TiO_2 catalyst shifted slightly higher binding energy side, showing the existence of positively charged Pt even after the reduction at 573 K. The TOFs of WGSR as well as CO–H_2 reactions were estimated from these dispersion values derived from the amount of CO adsorption.

3.2. *CO–H_2O (WGSR) as well as CO–H_2 reactions over Pt–TiO_2(nt) and Pt/SiO_2(imp)*

Fig. 4 shows the time courses of CO conversion as well the product formation in the WGS reaction at 373 K over Pt–TiO_2 nanotube and Pt/TiO_2 catalysts. Accompanied with the decrease of CO, equimolar amount of H_2 and CO_2 was formed in the CO–H_2O (10 Torr each) reaction. The vertical axis of the figure is normalized as the amount of product formed per surface Pt atoms (TOF; turnover frequency of the product formation). From this result, it is concluded that the nanotube catalyst exhibits two to three times larger TOF for water gas shift reaction than conventional impregnation catalysts.

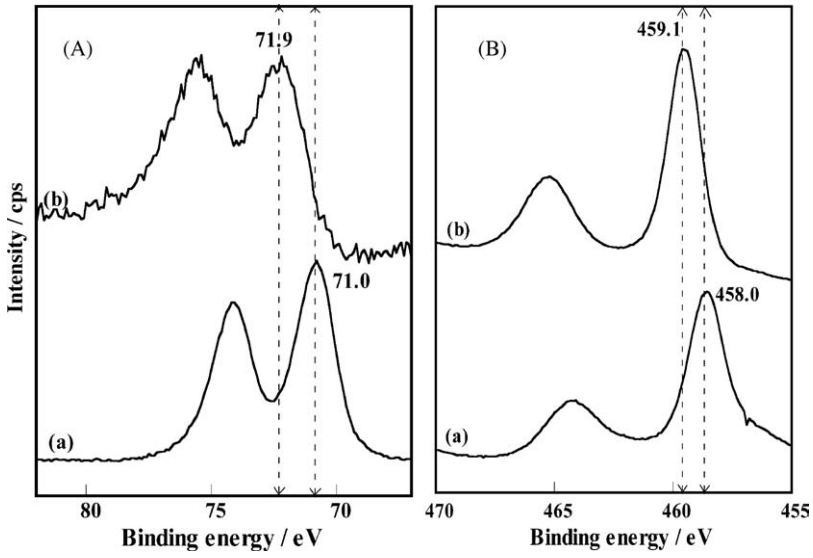

Fig. 3. XPS spectra of (A) Pt 4f and (B)Ti 2p transitions. (a) Pt–TiO_2(nt); (b) Pt/TiO_2(imp).

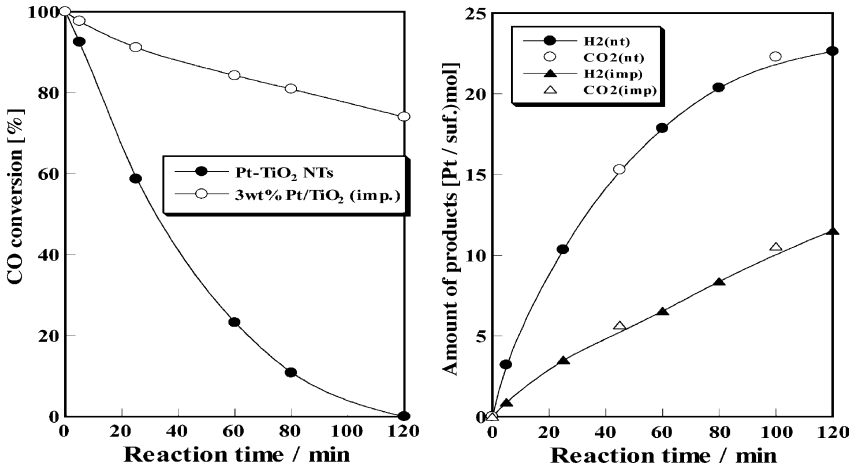

Fig. 4. Time courses of CO conversion as well the product formation in the WGS reaction at 373 K over Pt–TiO_2(nt) and Pt/TiO_2(imp) catalysts.

The WGS reaction is thought to occur mainly through two reaction mechanisms, the regenerative, redox mechanism and the associative mechanism [6,7]. The generative mechanism involves successive oxidation and reduction of the surface, while the associative mechanism involves reaction through an adsorbed surface intermediates, as a formate mechanism. The possibility of participation of carbonate and bicarbonate intermediate complexes instead of formats is also under discussion. In the formate mechanism, H_2O dissociation to form OH(a), which then reacts with CO to produce HCOO(a). Decomposition of formate then results in H_2 and CO_2 products. In the redox mechanism H_2O dissociates completely to O(a) and H(a) and the O(a) is then titrated by CO.

In the case of ceria catalysts loaded with reduction promoter metals [8–16], the ceria-mediated redox process has been proposed, whereby CO adsorbed on the metal is oxidized by ceria. The second step in the mechanism involves re-oxidation of ceria by water. Similar promotion effect of titanium oxide redox-cycle may be applicable in the present study. As already mentioned in the previous section, electron rich Ti^{3+} on the TiO_2 nanotube wall may play an important role to dissociate water molecule into OH(a) and H(a). The OH(a) may migrate to the Pt metal surface and oxidize CO molecule to form CO_2.

The temperature as well as pressure dependences of WGS reaction were shown in Fig. 5. From the Arrhenius plots of H_2 formation rates in Fig. 5(A), the activation energy of both catalysts were estimated as follows: 50.4 kJ/mol for Pt–TiO_2(nt) and 61.9 kJ/mol for Pt/TiO_2(imp). The pressure dependence of CO over both catalysts is shown in Fig. 5(B). The reaction order upon the partial pressure of CO was nearly zero in the case of impregnated Pt/TiO_2, while slightly positive order over Pt–TiO_2(nt), suggesting weakly adsorbed CO may easily be oxidized by OH(a) group.

Fig. 6 shows the time courses of CO–H_2 reaction over Pt–TiO_2(nt) and conventional impregnation catalysts. The rate of methane formation was two orders of magnitudes faster in the case of nanotube catalyst as shown in the figure. Methanol was also formed in both catalysts with the induction period of 30 min to 1 h, and the formation rate over former catalysts was two orders of magnitudes faster than the latter. Table 2 summarizes the selectivity of CO–H_2 reaction over both catalysts. In the case of nanotube catalyst, the selectivity for methanol formation at 393 K was only 17% after 4 h because of

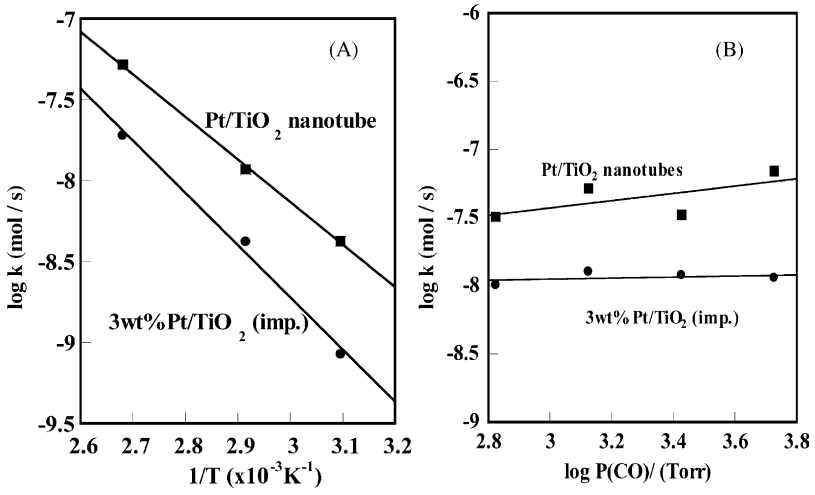

Fig. 5. Temperature and pressure dependences of WGS reaction over Pt–TiO_2(nt). (A) Arrhenius plots and (B) pressure dependence of COP(H_2O) = 10 Torr (const).

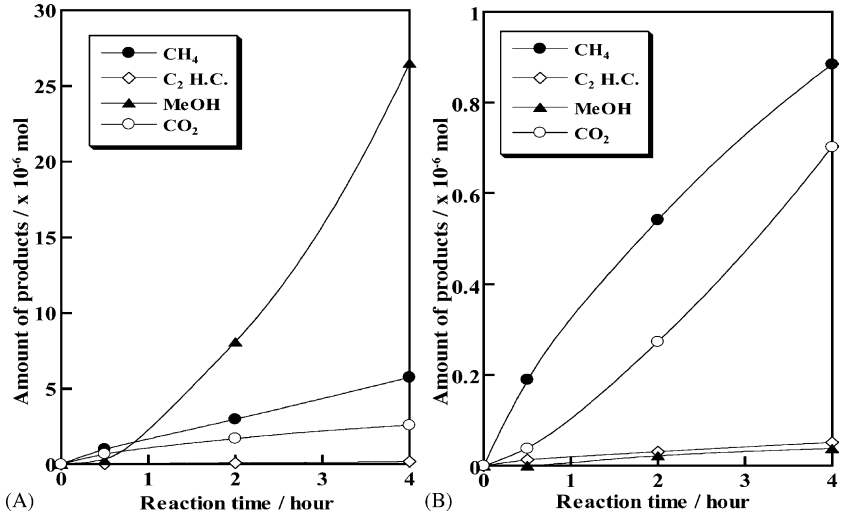

Fig. 6. Time courses of CO–H_2 reaction over (A) Pt–TiO_2(nt) and (B) Pt/TiO_2(imp) at 423 K.

the longer induction period at lower temperatures. At higher temperatures, methanol selectivity increased significantly, and around 80% selectivity was observed. As described in the previous section, similar promotion effect of Ti^{3+} species on the nanotube wall may be applicable for selective methanol formation, by supplying active OH(a). On the other hand, main product over impregnated catalysts was methane, whose formation rate was two orders of magnitude smaller than the nanotube catalysts.

3.3. In situ FT-IR study during the CO–H_2O and CO–H_2 reactions

Fig. 7 shows the FT-IR spectra of adsorbed CO onto the freshly reduced catalysts, followed by an evacuation at elevated temperatures. In the case of impregnated Pt/TiO_2(imp), a sharp band was observed at 2090 cm^{-1}, which can be assigned to a linearly adsorbed CO on top of the surface Pt atoms. After evacuation of the gas phase the temperature programmed desorption (TPD) experiment was carried out as summarized in Fig. 7(B). The intensity of the peak decreased gradually as the temperature was raised from 298 to 423 K, although the peak top position did not change at all. Most of the adsorbed CO desorbed at around 473 K.

Tanaka and White have reported the IR study of CO adsorption over Pt/TiO_2 catalyst [17]. They observed two kinds of linear CO species at 2094 and 2077 cm^{-1}, which were assigned as adsorption on Pt close-packed (terrace) sites and Pt open (step) sites, respectively. In addition, they observed a bridged CO species at 1854 cm^{-1}. They also observed the

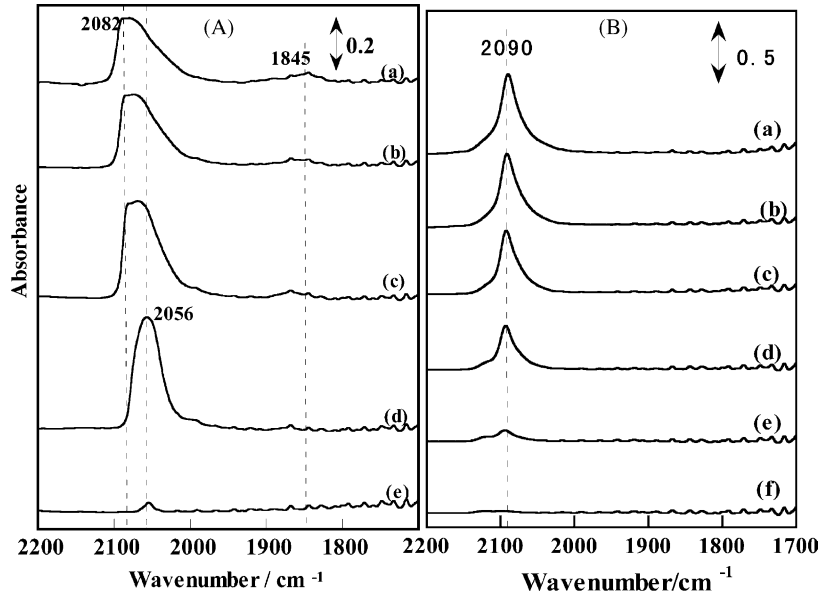

Fig. 7. FT-IR spectra of adsorbed CO over reduced (A) Pt–TiO_2(nt) and (B) Pt/TiO_2(imp) catalysts followed by TPD experiments. (A): (a) adsorption at 298 K followed by evacuation at (b) 298 K, (c) 373 K, (d) 473 K, and (e) 573 K. (B): (a) adsorption at 298 K followed by evacuation at (b) 323 K, (c) 373 K, (d) 423 K, (e) 473 K and (f) 523 K.

Table 2
Selectivity of CO–H_2 reaction over Pt–TiO_2(nt) and Pt/TiO_2(imp) catalysts (after 4 h)

Catalysts	Reaction temperature (K)	Selectivity (%)					
		CH_4	C2 HC	C3 HC	MeOH	EtOH	CO_2
Pt–TiO_2(nt)	393	77.4	4.9	0.3	17.1	0	0
	423	13.7	0.5	0.1	82.4	0.05	3.4
	453	16.4	0.5	0.1	75.5	0.09	7.4
Pt/TiO_2(imp)	393	87.8	12.2	0	0	0	0
	423	80.4	4.1	0	8.0	0	7.5
	453	52.6	3.1	0.3	2.3	0	41.8

lower frequency shift of 2094 cm^{-1} peak to 2078 cm^{-1} by TPD, which was attributed to the dipole–dipole interaction. The Pt metal dispersion of their sample was reported to be 0.2, which is quite different from our sample ($D = 0.58$, see Table 1).

In the case of Pt–TiO_2(nt), three CO(a) peaks were observed at 2082, 2060–2056 and 1845 cm^{-1}, which can be assigned to two linearly adsorbed CO and one bridged CO. By evacuation at 423 K, 2082 and 1845 cm^{-1} peaks behaved similarly and desorbed gradually from lower temperatures (spectra (c)). However, the CO(a) at 2056 cm^{-1} showed a very strong adsorption and stayed almost unchanged up to 473 K evacuation (spectrum (d)), which is completely different from Tanaka and White's result. Above 523 K the intensity of this peak decreased gradually indicating the desorption of adsorbed CO around these temperature ranges (500–550 K). These results indicate that the adsorbed CO at 2056 cm^{-1} in the nanotube is much stronger than CO(a) at 2090 cm^{-1} on the Pt/TiO_2(imp), showing a unique character of the Pt nanoparticles (bigger than 10 nm in size) on the inner surface of TiO_2 nanotube. Accordingly, it is reasonable to assign smaller Pt nanoclusters in the network of TiO_2 wall as the adsorption sites of CO(a) at 2082 cm^{-1}, which is opposite to Tanaka and White's conclusion.

Fig. 8 represents the FT-IR spectra during WGS reaction at 373 K. Over Pt–TiO_2 nanotube, adsorbed CO band shifted from 2082 to 2071 cm^{-1} during the reaction, accompanied with the appearance of a shoulder peak at 2025 cm^{-1} which disappeared quickly by gathering gas phase water into liquid N_2 cold trap. A large IR band at 1618 cm^{-1} can be assigned to adsorbed H_2O whose intensity also decreased by trapping gas phase with liquid N_2. In the case of impregnated Pt/TiO_2 during WGS reaction, linearly adsorbed CO band at 2090 cm^{-1} was also shifted to 2076 with a small shoulder at 2042 cm^{-1}, which also disappeared after liquid N_2 trapping. These results again suggest relatively weakly adsorbed CO may be responsible for WGS reaction.

The FT-IR spectra during CO–H_2 reaction at 423 K was summarized in Fig. 9. Over Pt–TiO_2 nanotube, two CO(a) bands were observed at 2080 and 1845 cm^{-1}, which may correspond to the highest and lowest frequency bands in Fig. 7. As the reaction proceeded, three new bands appeared at 1045,

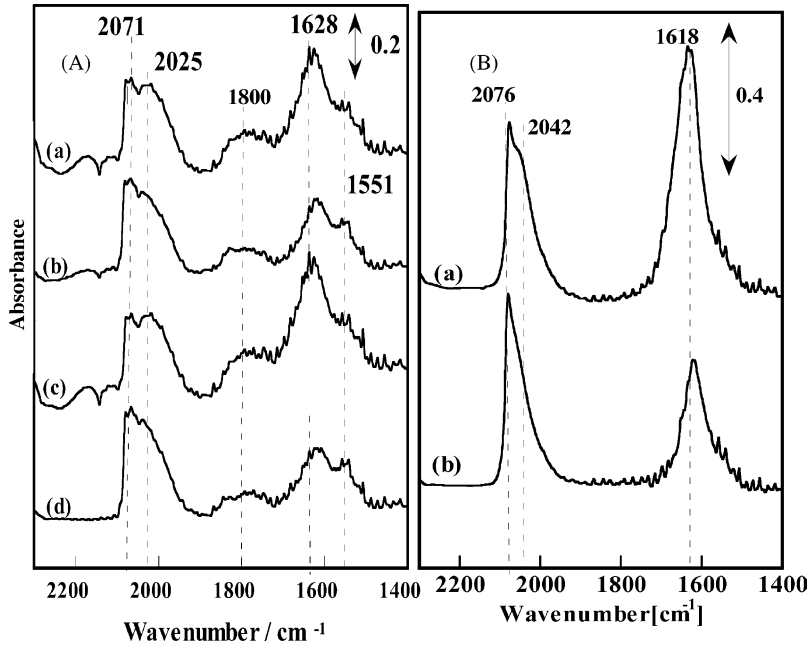

Fig. 8. FT-IR spectra of adsorbed species during WGS reaction at 373 K over (A) Pt–TiO_2(nt) and (B) Pt/TiO_2(imp) catalysts. (A): (a) WGSR at 373 K for 1 h, (b) liquid N_2 trap after (a), (c) WGSR at 373 K for 4 h and (d) liquid N_2 trap after (c). (B): (a) WGSR at 373 K for 2 h and (b) liquid N_2 trap after (a).

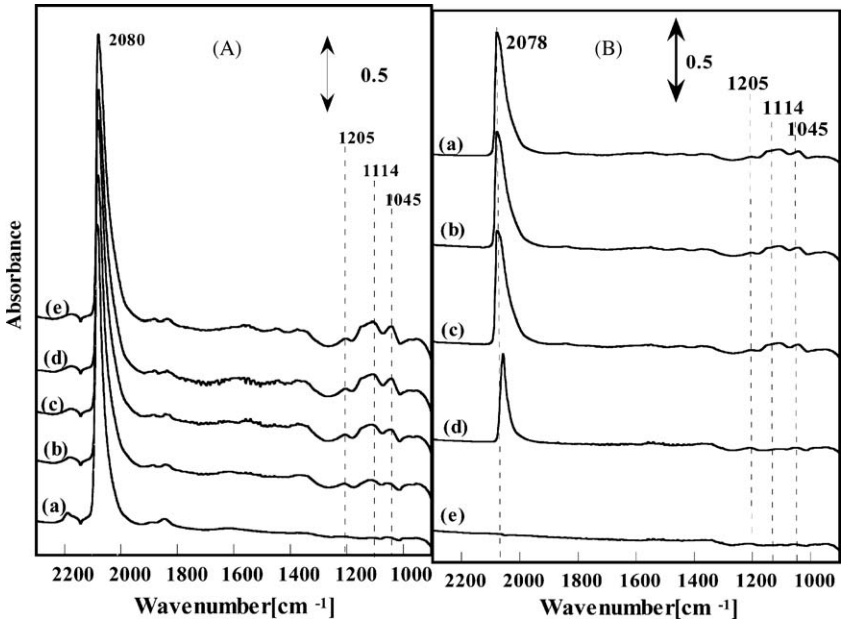

Fig. 9. (A) FT-IR spectra during CO–H_2 reaction at 423 K over Pt–TiO_2(nt). (B) TPR of adsorbed species after CO–H_2 reaction at 423 K over Pt–TiO_2(nt). (A): (a) 0 h, (b) 0.5 h, (c) 1 h, (d) 2 h and (e) 4 h. (B): (a) after 4 h CO–H_2 reaction, (b) H_2 at 298 K, (c) H_2 at 373 K, (d) H_2 at 473 K and (e) H_2 at 573 K.

1114, and 1205 cm^{-1} gradually, which can be assigned to surface methoxide and carbonate adsorbed species. After 4 h of the reaction the gas phase was replaced with H_2 at room temperature and TPR (temperature programmed reduction) experiment was continued. Adsorbed methoxide and carbonate peaks disappeared at around 423 K, suggesting the reaction intermediate-like behavior of these adsorbed species.

4. Conclusion

(1) The turnover frequency (TOF) of WGSR over Pt–TiO_2(nt) catalysts was two to three times larger than that over conventional impregnation Pt/TiO_2(imp) catalysts.
(2) The activity and selectivity for methanol in CO–H_2 reaction was extraordinary high in the case of Pt–TiO_2(nt) catalysts compared to the impregnation catalyst.
(3) The XPS and XRD analyses of the nanotubes revealed characteristic electronic state of reduced TiO_2 (Ti^{3+} in rutile structure) with zerovalent Pt even after the calcination at 773 K.
(4) In WGS reaction, electron rich Ti^{3+} on the TiO_2 nanotube wall may play an important role to dissociate water molecule into H(a) and OH(a), which may migrate to the Pt metal surface and oxidize CO molecule to form CO_2. In CO–H_2 reaction, similar promotion effect of Ti^{3+} species on the nanotube wall may be operating for selective methanol formation by supplying active OH(a).

Acknowledgement

This work was financially supported by High-Tech Research Center Project from the Ministry of Education Science, Sports and Culture.

References

[1] G.R. Patzke, F. Krumeich, R. Nesper, Angew. Chem. Int. Ed. 41 (2002) 2446.
[2] S. Naito, M. Ue, S. Sakai, T. Miyao, Chem. Commun. (2005) 1563.
[3] T. Miyao, T. Saika, Y. Saito, S. Naito, J. Mater. Sci. Lett. 22 (2003) 543.
[4] C. Hippe, M. Wark, E. Lork, G. Schulz-Ekloff, Microporous Mesoporous Mater. 31 (1999) 235.
[5] M. Wark, C. Hippe, Schultz-Ekloff, Stud. Surf. Sci. Catal. 129 (2000) 475.
[6] D.G. Rethwich, J.A. Dumesic, Appl. Catal. 21 (1986) 97.
[7] C. Rhodes, G. Huchings, A.M. Ward, Catal. Today 23 (1995) 43.
[8] G.S. Zafiris, R.J. Gorte, J. Catal. 139 (1993) 561.
[9] T. Shido, Y. Iwasawa, J. Catal. 141 (1993) 71.
[10] J. El Fallah, S. Boujana, H. Dexpert, A. Kiennemann, J. Majerus, O. Touret, F. Villain, F. Le Normand, J. Phys. Chem. 98 (1994) 5522.
[11] T. Bunluesin, H. Cordatos, R.J. Gorte, J. Catal. 157 (1995) 222.
[12] S.H. Overbury, D.R. Huntley, D.R. Mullins, G.N. Glavee, Catal. Lett. 51 (1998) 133.
[13] T. Bunluesin, R.J. Gorte, G.W. Graham, Appl. Catal., B 15 (1998) 107.
[14] A. Holmgren, B. Andersson, D. Duprez, Appl. Catal., B 22 (1999) 215.
[15] S. Hilaire, X. Wang, T. Luo, R.J. Gorte, J. Wagner, Appl. Catal., A 215 (2001) 271.
[16] Y. Li, Q. Fu, M. Flytzani-Stephanopoulos, Appl. Catal., B 27 (2000) 179.
[17] K. Tanaka, J.M. White, J. Catal. 79 (1983) 81.